Fenton Catalytic Properties of FeOOH Nanoparticles Dispersed on Volcanic Ash Activated by Gliding Arc Plasma

Mélanie Pitap-Mbowou[a], Franck W. Boyom-Tatchemo*[a], Francois Devred[b], Georges Kamgang-Youbi[a], Elie Acayanka[a], Renaud Cousin[C], Eric M. Gaigneaux*[b], Samuel Laminsi[a]

[a] Mrs. M.M. Pitap, Dr. F. W. T. Boyom, Prof. G. Y. Kamgang, Prof. E. Acayanka, Prof. S. Laminsi
Department of inorganic Chemistry
University of Yaounde I
B.P.812, Yaounde, Cameroon
E-mail: (Franck W. Boyom-Tatchemo) boyom.william@yahoo.com

[b] Dr. F. Devred, Prof. E. M. Gaigneaux
Institute of Condensed Mater and Nanosciences-IMCN, Division "Molecular Chemistry, Materials and Catalysis-MOST", Université catholique de Louvain,
Place Louis Pasteur 1/L4.01.09.1348 Louvain -la-Neuve, Belgium
Email : eric.gaigneaux@uclouvain.be,

[c] Prof. R. Cousin
Unité de Chimie Environnementale et Interactions sur le Vivant-UCEiV, UR4492
Université du Littoral Côte d'Opale
145 avenue Maurice Schumann 59140, Dunkerque, France

Corresponding authors: Franck W. Boyom-Tatchemo (boyom.william@yahoo.com); (Eric M. Gaigneaux) (eric.gaignaux@uclouvain.be)

Abstract:

We explore two approaches for preparing supported catalysts based on volcanic ash (VA) as support for effective Fenton heterogeneous catalysis. Firstly, the plasma-deposition of FeOOH (goethite) on VA activated chemically by HCl (AM-FeOOH-30/0C) was performed. Secondly, the plasma-activation of VA and -deposition of FeOOH (VA-FeOOH-30/0) were carried out simultaneously, taking advantage of the gliding-arc-plasma acidic and oxidizing properties. Prepared materials were characterized by X-ray diffraction (XRD), Fourier-transform infrared spectroscopy (FT-IR), thermogravimetric analysis (TGA), N_2 physisorption, and scanning electron microscopy coupled energy-dispersive X-ray spectroscopy (SEM/EDX). Performing chemical activation of VA using HCl induces a better microstructure's modification (specific surface area and porosity) and allows a better plasma-deposition of FeOOH (AM-FeOOH-30/0C) compared to performing both processes simultaneously by plasma (VA-FeOOH-30/0) which did not change its microstructure, but slightly improved the texture. Otherwise, ageing (plasma post-discharge treatment) of AM-FeOOH-30/0C material induces crystallite's nucleation, thus an increase of the specific surface area (AM-FeOOH-30/4C). Fenton catalytic degradation of Rhodamine-6G (25 mg/L) for 20min revealed elimination degrees of 22, 87, 78, and 82% respectively for VA-FeOOH-30/0, AM-2C, AM-FeOOH-30/0C, and AM-FeOOH-30/4C materials. The recyclability tests confirmed the higher catalytic stability of AM-FeOOH-30/0C compared to VA-FeOOH-30/0 material after 4 cycles, thus highlighting the necessity to perform the activation and deposition separately.

1. Introduction

Optimizing the properties of Fenton's heterogeneous catalysts such as activity, selectivity, and catalytic/thermal stability remains nowadays a major challenge for researchers [1, 2]. Therefore, FeO_x is the common catalyst used during Fenton's heterogeneous catalysis for an effective organic pollutant's removal, due to its easy use, low cost, and a large production of oxidizing species such as hydroxyl radical (HO•) via decomposition of H_2O_2 [1]. To ensure the long-life cycle of the catalyst, Fenton's heterogeneous catalysis was developed via the deposition of FeO_x (active phase) on the suitable support to address the issue of iron leaching, Fenton's homogeneous catalysis producing sludge, which complicated catalyst recovery and requires further treatment of the effluent before the release into the environment [3-8]. Preparing supported-FeO_x will limit the particle's agglomeration on the one hand, and allow the ability to carry out the Fenton catalytic route in a large pH range on the other hand. However, it is known that FeO_x particles have a very strong affinity for micrometrical sized supports and aluminosilicate-rich solids such as zeolites, clays, laterite and silica [9-15]. These supports are known as inhibitory sources of iron oxides (FeO_x) leaching in aggressive aqueous solution, through its good dispersion (deposition) on their surfaces [16-18]. Other authors in their respective works have shown that Goethite (FeOOH) supported on amorphous silica has more active layers than that of hematite (Fe_2O_3) [1, 14, 15].

Cameroon is full of volcanic ash deposit sites largely available (free access). Volcanic ash has a rigid aluminosilicate framework, high thermal stability and non-negligible of Fe-content [6, 19], making that it could be used as a good catalyst support for a better stability of the active phase (FeO_x) during the catalytic route in liquid phase. In addition to play the catalytic support role, VA could actively participate to the catalytic process as it contains Iron-compound within its structure. Unfortunately, this local material reveals some drawbacks such as a low specific surface area and porosity, thus limiting its surface energy and the accessibility to their active sites. Therefore, a prior surface activation (modification) of raw VA remains a necessity. In our recent work, we have shown that the chemical activation of volcanic ash (VA) using sulfuric acid (H_2SO_4) could be inhibited by the formation of calcium sulphate ($CaSO_4$), inducing the clogging of pores, likely to weaken the plasma-deposition of FeO_x, thereby reducing the catalyst reactivity [1]. To solve this, we intend to use in the present work hydrochloric acid (HCl) as activating agent, following some literature works which showed that the chemical activation of VA using HCl allows a better removal of the impurities, basic phases and avoids the formation of undesirable products such as $CaSO_4$ as when sulfuric acid is used [18, 19]. Otherwise, knowing that Glidarc plasma route operates in mild conditions (atmospheric pressure and ambient temperature), it generates electroshock waves, UV-visible light, acid (HNO_2 and HNO_3) and redox (HO•, NO•, NO_2^-, or NO_3^-) species in the core of the reactor [2, 12, 20-28]. Therefore, the generated photons and species could allow the simultaneous plasma-activation of VA and plasma-deposition (precipitation) of FeOOH through oxidation of Fe^{2+} solution without adding any extra chemical reagent. This would bring more simplicity to the activation and deposition processes, by reducing operating time, limiting the use of chemical products, which could be economically beneficial.

The aim of this study consisted in assessing the effect of the VA activation route on the plasma-deposition efficiency of FeOOH. The first route consisted in carrying out the chemical activation of VA using hydrochloric acid (HCl) and comparing the materials obtained with those when H_2SO_4 is used as activating agent [1], followed by glidarc plasma-deposition of FeOOH. To better appreciate the possibility of reducing the operating time and energy related to the chemical activation of VA as a catalytic support, followed by glidarc plasma-deposition of FeOOH (active phase) on the chemically activated support, the second route consisted in performing both processes simultaneously by glidarc plasma. In our previous work [26], we showed that the ageing (glidarc plasma post-

discharge treatment) of bulk plasma precipitated MnO_2 significantly changes its crystalline structure, morphology and increases the specific surface area, which changes are ascribed to the evolution of the crystallite's nucleation thanks to reactive species such as H_2O_2, HNO_3 generated after extinction of the plasma discharge (plasma post-discharge reactions) [26]. Recently, we explored the effect of these plasma post-discharge species on the FeOOH plasma-deposited on VA chemically activated using H_2SO_4 and recorded a significant decrease of the specific surface area of the deposited material after ageing, which is ascribed to the deposition of FeOOH inside the pore [1]. This is why, in the present work, we intended to assess the effect of the VA activating agent by using HCl, on the nucleation process (during the ageing) of plasma-deposited FeOOH. Afterwards, the Fenton catalytic activity and recyclability tests of prepared materials have been assessed during the degradation of Rhodamine-6G as the organic pollutant model.

2. Material and methods

2.1. Material

The volcanic ash (VA) used in this investigation was supplied by MIPROMALO (Mission for the Promotion of Local Materials in Cameroon) and was extracted from Foumbot in the Western Region of Cameroon. Rhodamine-6G (Rh-6G) was purchased from Sigma-Aldrich in Belgium, with the physicochemical properties summarized in Table S_1. Hydrochloric acid HCl (37%) and sodium hydroxide NaOH (100%) were purchased from Sigma-Aldrich. Heptahydrated Iron (II) sulphate $FeSO_4.7H_2O$ as synthesis precursor of FeOOH particles, and hydrogen peroxide (H_2O_2, 50%), were purchased at Merck company.

2.2. Preparation of supported catalysts

The supported catalysts were prepared following the protocol established in the previous work [1], while replacing H_2SO_4 by HCl as activating agent of the VA. This consisted in washing raw volcanic ash (VA) with distilled water to remove soluble contaminants, then drying at room temperature for three days before being crushed and sieved at 100 µm. Afterwards, the chemical activation of VA was carried out by adding 10g of cleaned VA to 100 mL of hydrochloric acid (3M) in a boiling water bath (100°C), and mechanically stirring at 500 rpm for two hours. The final product was vacuum-filtered, cleaned with hot distilled water to achieve neutral pH, dried for 3h at 105°C in an oven and named AM-2C. The plasma-deposition of FeOOH on the chemical activated VA using HCl and the ageing process were carried out following the protocol of the previous work [1]. Therefore, a mixture of $FeSO_4.7H_2O$ solution (0.5 g/L, 430 mL) and 4g of AM-2C material was exposed to glidarc plasma treatment for 30 min, and the obtained yellow-brown precipitate was recovered. While the ageing consisted in exposing the deposited precipitate in a boiling water bath (100°C) for 4h under mechanical agitation to pursue the eventual nucleation (maturation) process of the crystallites. Both products resulting from the plasma-deposition and ageing processes were washed using distilled water, dried in oven at 105°C for 24h and respectively named AM-FeOOH-30/0C and AM-FeOOH-30/4C. As a comparison to previous process, simultaneous plasma-activation of VA and plasma-deposition of FeOOH was performed. It consisted in exposing for 30 min the mixture of raw VA (4g) and 0.5 g/L of Iron (II) solution (430 mL). Afterwards, the recovered final product (without ageing), was washed, dried in an oven at 105°C for 24h and named (VA-FeOOH-30/0).

2.3. Characterization of obtained materials.

X-ray diffraction patterns of prepared materials were recorded from 5 to 80 degrees (2theta) with an increment of 0.015 degree and integration time of 0.15 second using a Bruker Advance diffractometer equipped with a LynxEye XE-T detector. The analysis was operated at 40 kV and 30 mA, using Cu K_α radiation (0.15418 nm). The powdered samples were dispersed on zero background type sample holder (silicium chip). The crystalline phases were identified using the ICDD-JCPDS database. The nitrogen physisorption analyses were performed using a Micromeritics Tristar 3000 analyzer by adsorption of nitrogen (N_2) at a temperature of 77 K, in a relative pressure P/P◦ range of 0 to 0.98. Before the analysis, a vacuum pre-treatment of the samples was carried out at 150°C for 12 hours. The specific surface area was calculated using the Brunauer, Emmet, and Teller (BET) technique and adsorption-desorption isotherms. The pore size distribution was extracted from the desorption branch using the Barrett-Joyner Halenda (BJH) technique. t-plot approach was used to determine the non-porous surface and microporous volume [29]. Fourier transform infrared spectroscopy was performed in Total attenuated reflectance mode performing after 32 scans at a resolution of 4 cm^{-1} in the wavelength range of 4000-400 cm^{-1} using an Invenio S spectrometer (Bruker) equipped with a Platinum ATR platform coupled with a DLaTGS detector. The atmospheric air spectrum was used as a reference and was subtracted from the material spectrum recorded. To find the degradation temperature of each material, TGA analysis was performed using Mettler Toledo TGA/SDTA 851 TA Instruments SDT 290 thermo-analyzer, using air (100 mL/min) within the temperature range of 25-900°C, at a heating rate of 10°C/min. SEM coupled to EDX analysis were carried out using a LEO 983 GEMINI electron microscope operated at an acceleration voltage of 2 kV, to get the morphology of particles and elementary composition at the surface of each material. Before performing SEM and EDX analyses, a small quantity of material powder is placed on adhesive carbon film which is itself deposited on an aluminium support. Afterwards, 8 nm layer of chromium or gold is sputtered under vacuum with a sputter Metal 208HR (Cressington). The elementary composition of each material was calculated by removing the carbon and chromium (or gold) contribution, and then bringing the remaining to 100%. This was made at three different points for each sample made and the average value calculated from these analyses are reported. The zero-charge point of prepared materials was determined using method of *Bailed et al.* [1, 30]. Therefore, 0.1g of VA, AM-2C, VA-FeOOH-30/0, AM-FeOOH-30/0C or AM-FeOOH-30/4C material was introduced into flasks containing 0.5 L of NaCl solution (0.01M). The solutions were adjusted to different pH values (2, 4, 6, 8 and 10) using HCl (0.01M) or NaOH (0.01M). The different mixtures were kept under magnetic stirring for 48 h. After 5 minutes of centrifugation at 3600 rpm, the final pH of the supernatants was measured. The intercept of the curve at initial pH equal to final pH on the plot represents the point of zero-charge (PZC) of each material.

2.4. Fenton catalytic tests of different materials.

Catalytic Fenton treatment of Rhodamine-6G solution (25 mg/L) was carried out at ambient temperature (25 ± 3°C), under the optimal conditions obtained in the previous work (pH=7, t=20 min, m=3 g/L, and 1 mL of H_2O_2) [1]. At pH=7, the values of PZC of the materials resulting from the VA recorded in the present work (section 3.1.) which are lower than those obtained in our previous work [1], promote a better adsorption process, and thus induce a better catalytic process. The catalytic tests of VA, AM-2C, VA-FeOOH-30/0, AM-FeOOH-30/0C or AM-FeOOH-30/4C materials and post-catalytic treatment (to better assess the degradation process of Rhodamine-6G), analysis of different solutions, recyclability study of each material and leaching tests of Iron were described in our previous work [1]. The degradation degree (T%) of Rh-6G was determined using the equation 1, where C_0 and C_f represent

respectively the initial and residual concentration of the pollutant solution before and after treatment at defined time. Moreover, to have a deep understanding of the catalyst's structural stability after the catalytic reaction, VA-FeOOH-30/0, AM-FeOOH-30/0C materials have been recovered after the first catalytic cycle and characterized by XRD and FTIR analysis as previously described.

$$T\% = \frac{C0 - Cf}{C0} * 100 \quad (1)$$

3. Results and Discussion

3.1. Characterization of prepared materials

X-ray Diffraction (XRD)

The X-ray diffraction patterns and contained phases of raw volcanic ash before (VA, Fig. 1a) and after chemical activation using HCl (AM-2C, Fig. 1b), of materials resulting from the activation of VA and deposition of FeOOH simultaneously by plasma (VA-FeOOH-30/0, Fig. 1c), and of materials resulting from plasma-deposition of FeOOH on chemical activated VA (AM-FeOOH-30/0C, Fig. 1d), eventually followed by the ageing (AM-FeOOH-30/4C, Fig. 1e) are presented in Fig. 1 and Table S_2. The XRD pattern of the raw volcanic ash (VA) already recorded in previous works [1] revealed disordered Sodium Anorthite (Ca, Na) $(Si, Al)_4O_8$ (PDF : 00-041-1481), Augite $Ca(Mg_{0.7}Al_{0.30})(Si_{1.7}Al_{0.30})O_6$ (PDF : 01-078-1392), Maghemite Y-Fe_2O_3 (PDF : 00-039-1346), Hematite-Fe_2O_3 (PDF : 00-033-0664), Wuestite FeO (PDF : 01-089-2468), Silicon Oxide-SiO_2 (PDF : 00-050-1708), and Ferroan Forsterite $Mg_{1.824}Fe_{0.176}(SiO_4)$ (PDF : 01-083-1541). The chemical activation using hydrochloric acid revealed the same phenomenon and phases as those recorded when sulfuric acid had been used [1], as the disappearance of ferric forsterite, maghemite, hematite and wuestite phases due to the exposure of VA to an acidic medium which induces the leaching of iron (Eq. 2) [31, 32]. However, the use of hydrochloric acid induces the formation of a dome between 20 and 30° on the AM-2C pattern indicating the formation of an amorphous phase within the geopolymer [1, 33, 34]. According to *Duxson et al. (2007),* geopolymerization determines the microstructure and pore distribution of the material, which are essential for textural properties of the material [35]. Therefore, activation of VA using HCl could develop more pores, a larger specific surface area, and the formation of a more reactive three-dimensional amorphous aluminosilicate framework compared to the material resulting from the H_2SO_4 activation [1]. AM-2C (Fig. 1b) material exhibits much more amorphous phase than the material (AM-2) obtained after activation of VA using H_2SO_4 [1]. Plasma-deposition of FeOOH on the HCl activated chemically VA induces the formation of new phases, notably labradorite $Ca_{0.68}Na_{0.30}(Al_{1.66}Si_{2.34}O_8)$ (PDF : 01-083-1372), Augite Aluminate Ca (Mg, Fe, Al)(Si, $Al)_2O_6$ (PDF : 00-041-1483), and a slight increase of the dome intensity between 20 and 30°, proving that AM-FeOOH-30/4C has a larger amount of amorphous phase. These results highlight the fact that iron oxide nanoparticles plasma-deposited on VA chemically activated is in the form of amorphous goethite (FeOOH) with orthorhombic lattice, embedded in amorphous aluminosilicate and aluminate augite phases present within VA. In contrast, the material resulting from the simultaneous plasma-activation of VA and plasma-deposition of FeOOH does not reveal any modification of the crystalline phases of VA. No new mineral phases appear on the pattern, which proves that the activation of VA and deposition of FeOOH simultaneously by glidarc plasma does not lead to any change of the VA microstructure. Therefore, chemical activation of VA with hydrochloric acid deeply facilitates the modification of VA microstructure and better plasma-deposition (dispersion) of FeOOH compared to the simultaneous plasma-activation of VA and -deposition of FeOOH. The mechanism of chemical activation of VA

using HCl is described according to equation 2. Following the acid-base properties of main components within the raw VA, CaO (basic oxide), Al_2O_3 and Fe_2O_3 (amphoteric oxides) react with hydrochloric acid (HCl), while SiO_2 (acidic oxide) does not react. The mechanism of Glidarc Plasma activation of VA consists in chemical and physical attacks. The chemical attack is based on acid-base reactions as previously described (Eq.2) knowing that plasma medium generated strong acidic species such as HNO_2 and HNO_3. While the physical attack of VA consists in bombarding VA surface by high-energy electrons, reactive species, and plasma-emitted shock waves, inducing the disaggregation of the particles, which may increase the specific surface area and porosity. Furthermore, the Si-O-T (Al, Si, Fe) bridges are broken, generating ≡Si-OH, ≡Al-OH, ≡FeOOH and modifying the microstructure of the VA. Otherwise, ≡Si-OH reacts with iron ion from $FeSO_4.7H_2O$ precursor to form ≡Si-O-Fe and ≡Al-O-Fe bonds, thus increasing the surface acidity. For plasma-deposition of FeOOH on the activated VA, plasma-generated oxidizing species (HO•, H_2O_2, etc.), oxidize Fe^{2+} from the precursor, leading to the precipitation of FeOOH on the VA surface/lattice. However, despite the quasi similarity of AM-FeOOH-30/0C (Fig. 1d) and AM-FeOOH-30/4C (Fig. 1e) diffractograms, we can remark that some peaks intensity changes after the ageing process. These changes are ascribed to the evolution of the crystallite's nucleation (maturation). Around 37° (Fig.1), the broad peak is narrowing with a slight intensity increase, thus highlighting the formation of new phases after the ageing. The ageing of the plasma-deposited material (AM-FeOOH-30/0) in boiling water bath leads to the formation of andesine, a silicate mineral member of the plagioclase and feldspar group which is located within the middle of this series and is characterized by an equal percentage of sodium and calcium in its composition. This further highlights the structural modification and evolution of the crystallite's nucleation during ageing at plasma post- discharge.

$$zSiO_2, yFe_2O_3, xAl_2O_3, nCaO + 2(3y + 3x + n)HCl \rightarrow zSiO_2 + 2x\,AlCl_3 + 2yFe\,Cl_3 + nCaCl_2 + \\ + (3y + 3x + n)H_2O \qquad (2)$$

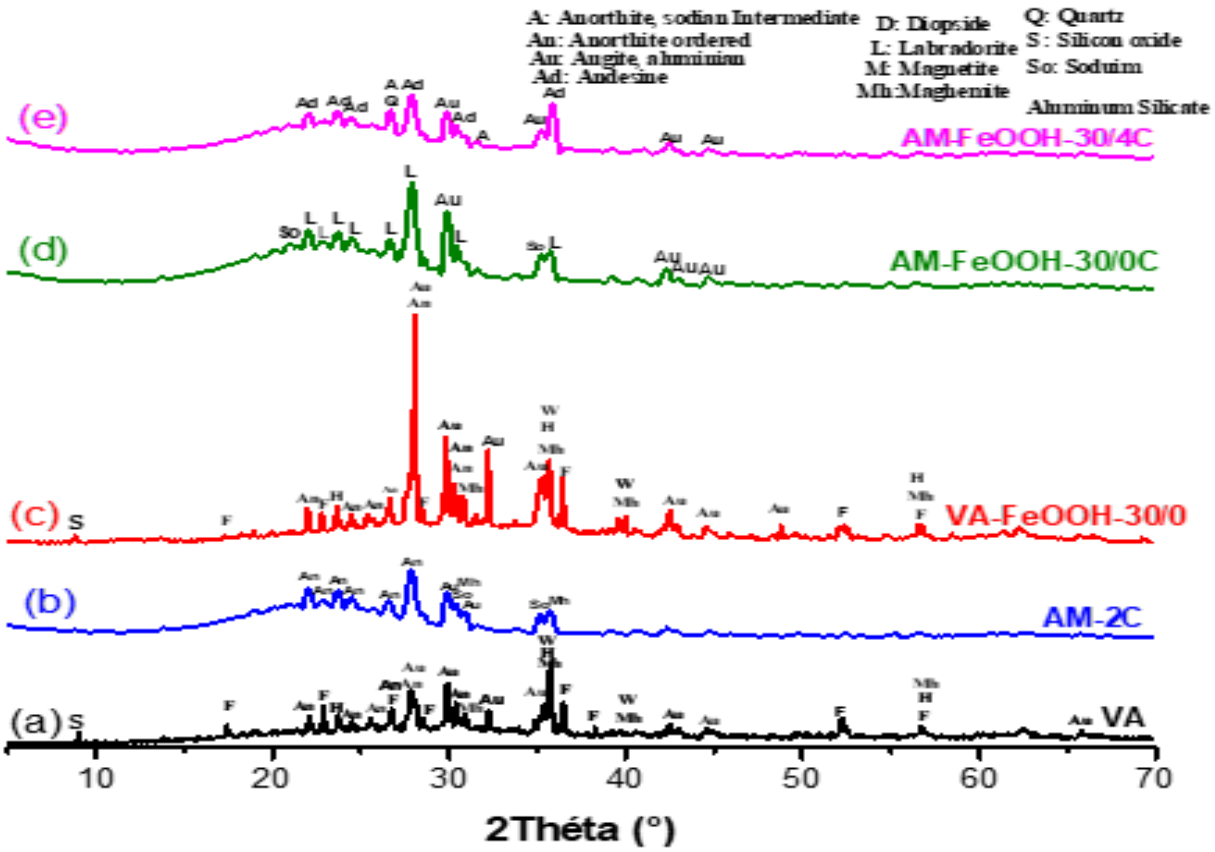

Figure 1. XRD patterns of (a) Raw VA, (b) Activated (AM-2C); (C) activated VA and deposited FeOOH simultaneously by plasma (VA-FeOOH-30/0) (d) Chemical activated VA and deposited FeOOH by plasma (AM-FeOOH-30/0C), (e) Ageing AM-FeOOH-30/4C materials.

Fourier Transform Infrared Spectroscopy (FTIR)

Fig. 2 depicts the FTIR spectra of different materials. The symmetric stretching vibration of Si-O-T bonds (where T=Si, Al) is represented by a large absorption band around 913 cm^{-1} in the raw volcanic ash (VA) [1, 36]. After chemical activation using hydrochloric acid (AM-2C), absorption bands are observed around 3346 and 1612 cm^{-1} corresponding respectively to the stretching and bending vibrations of the OH group from physisorbed and chemisorbed water molecules contained in the amorphous phase as previously revealed by the XRD pattern of AM-2C material. Moreover, we observe the shift of the absorption band from 913 to 954 cm^{-1} and the appearance of the deformation vibration band around 1057 cm^{-1}, all corresponding to the vibration mode of the Si-O-T bonds (T = Si, Al, Fe). This shift of the absorption band can be explained by the structure modification within the material through geopolymerization, which leads to the partial replacement of SiO_4^- by AlO_4^- tetrahedra within the framework of VA. We also observe an absorption band around 793 cm^{-1} on the AM-2C spectrum's corresponding to the vibration mode of the α-Fe-O-OH groups of goethite. The band around 534 cm^{-1} corresponds to the vibration modes of the Al-O bond with Al in hexacoordinate coordination, and the one appearing around 433 cm^{-1} attests the presence of Fe^{3+}. The plasma-deposition of FeOOH on the aluminosilicate framework of VA activated by HCl, leads to a decrease of the absorption bands intensities around 1052 and 953 cm^{-1}. This may indicate a diminution of the 3D aluminosilicate network due to the substitution of Al by Fe atoms and confirms the above-mentioned statements (XRD analyses), suggesting that α-FeOOH would be embedded in the amorphous aluminosilicate phase of activated VA. Furthermore, the plasma-deposition of FeOOH nanoparticles, followed by ageing process, induces appearance of a new absorption band around 668 cm^{-1} corresponding to the symmetric stretching vibration mode of Si-O-Fe bond [37]. Regarding the spectrum of VA-FeOOH-30/0 resulting from the activated VA and deposited FeOOH simultaneously by glidarc plasma, the formation of a new band around 694 cm^{-1} is attributed to the deformation vibration of Si-O-Al bonds and shows that Al, initially in coordination IV, has been transformed into coordination VI within the framework [38]. A new adsorption band appears around 610 cm^{-1}, corresponding to the deformation vibrations of Si-O-Al and Si-O-Si bonds characteristic of geopolymer materials [39]. The increase of the absorption bands width around 3346 cm^{-1} corresponds to the grafting of hydroxyl groups HO• (generated in the core of the plasma reactor) onto the material surface and the formation of silanol and aluminol groups. This suggests that the chemical environment of Si-O-Al has been modified with the formation of silanol within the framework, inducing an incomplete geopolymerization of the material with an increase and a shift of a broad absorption band from 913 to 1048 cm^{-1}. The presence of silanol into the structure highlights the fact that activation of volcanic ash and simultaneous deposition of FeOOH by plasma do not change the microstructure of VA and corroborates what was previously revealed by XRD.

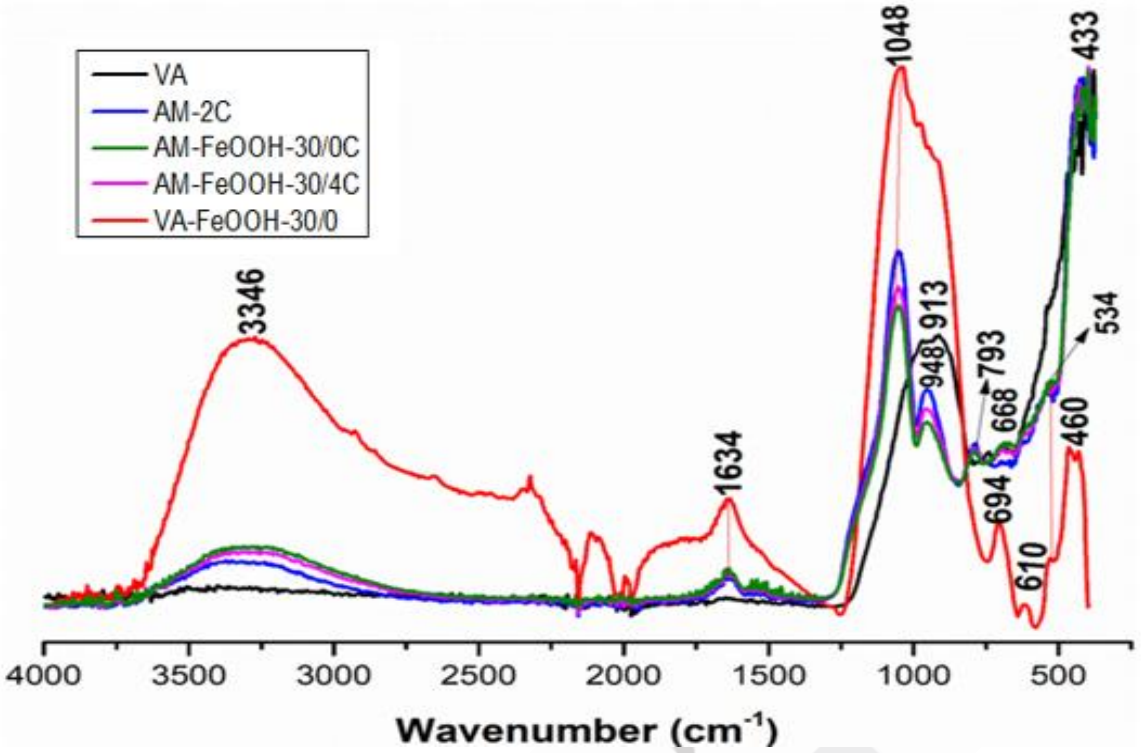

Figure 2. Infrared spectra of Raw VA, activated (AM-2C), activated VA and deposited FeOOH simultaneous by plasma (VA-FeOOH-30/0), Chemical activated VA and deposited FeOOH by plasma (AM-FeOOH-30/0C) and Ageing AM-FeOOH-30/4C materials.

Thermal analysis

Fig. 3 shows the TGA thermograms and DTG curves of VA, AM-2C, AM-FeOOH-30/0C, and AM-FeOOH-30/4C and VA-FeOOH-30/0. Raw volcanic ash (VA) shows one mass loss of 1.3% between 25 and 100°C, corresponding to the dehydration of free or physisorbed water (Fig. 3a). For chemical activated material AM-2C, a total mass loss of 9.6% is observed on the thermogram (Fig. 3a), and the formation of a single endothermic peak around 70°C on the DTG curve is recorded (Fig. 3b), corresponding to the dehydration of free water (Fig. 3b) [40, 41]. Therefore, chemical activation of VA using HCl increases the amount of chemical and physical bound water compared to when sulfuric acid is used [1]. This could be ascribed to the huge pores opening within AM-2C material as attested by N_2 physisorption analysis (see next section). This is in accordance with the work of *Otieno et al. (2023)* on the zeolite synthesis, which shows that activation of tropical VA using HCl increases the mass loss percentage [31]. The plasma-deposition of FeOOH on the AM-2C surface without ageing induces an increased mass loss (11.7%), which shows that the dehydration process of the AM-FeOOH-30/0C material (Fig. 3) occurs slowly in a single step and can be explained by the increase of amorphous phase within the material. Furthermore, it can also be explained by the grafting of hydroxyl groups (HO•) produced by glidarc plasma into the cavities and on the material surface. *Tiya et al. (2015)* reported that exposing Fe^{2+} salt hexahydrated to glidarc plasma induces the formation of goethite (FeOOH), undergoing a dehydration around 250-350°C with a mass loss of 11.5% and the occurrence of an endothermic phenomenon [28]. In the present work, the use of Fe^{2+} heptahydrated as a precursor for the plasma-deposition of FeOOH on activated volcanic ash (AM-2C) does not induce this phenomenon, even the same mass loss was reached (11.7%). This indicates that α-FeOOH fixed on the chemical activated volcanic ash, is embedded into the amorphous 3D aluminosilicate phase. On the other hand, the VA-FeOOH-30/0 material (Fig. 3a) is thermally stable and exhibits a low mass loss (3.7%) with a single endothermic

phenomenon (Fig. 3b) between 25 and 85°C corresponding to the removal of a little amount of physical bound water. These results deeply confirm the earlier statements that simultaneous plasma-activation of VA and -deposition of FeOOH do not modify the microstructure of the VA. The ageing of the material resulting from the plasma-deposited FeOOH on chemical activated VA (Fig. 3a) leads to an increase in mass loss and the disappearance of the endothermic peak (Fig. 3b). The recorded mass loss of 13.2% can be attributed to the removal of adsorbed water and the dehydroxylation of Goethite, thus confirming the previously mentioned assertions that ageing would lead to the development of goethite crystals on the material surface and induce the opening of pores, hence the increase of the specific surface area. Additionally, the increase of the mass loss may also be attributed to the growth of the amorphous phase within the material. Therefore, the mass losses between 350-450°C and 450-600°C for AM-FeOOH-30/0C material could respectively be ascribed to the transformation of goethite to hematite and reduction of magnetite to Wuestite.

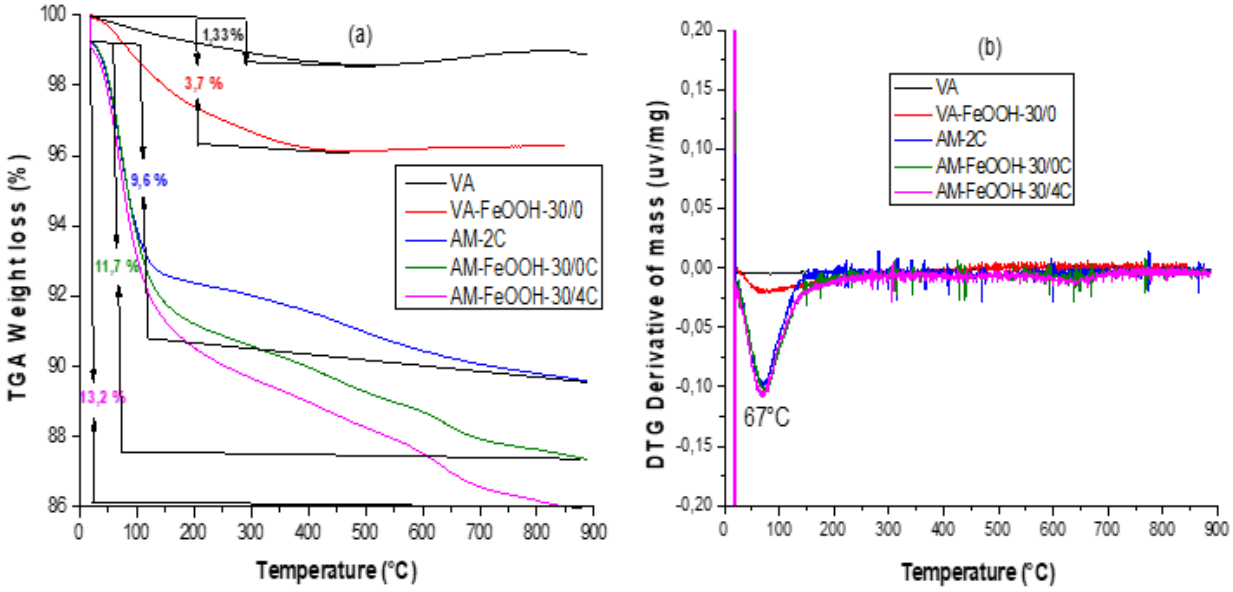

Figure 3. TGA (a) and DTG (b) curves of Raw VA, activated (AM-2C), simultaneous plasma activated VA and deposited FeOOH (VA-FeOOH-30/0), chemical activated VA and plasma deposited FeOOH (AM-FeOOH-30/0C) and Aged AM-FeOOH-30/4C materials.

Nitrogen physisorption

Fig. 4 presents the adsorption-desorption isotherms of different obtained materials. It emerges that the raw volcanic ash (VA) exhibits type IV isotherm with a hysteresis loop weakly marked at high relative pressure, illustrating the presence of weak mesoporosity between particles and bottle-shaped pores with necks of very disparate size and bottle bottoms with more homogeneous sizes (Fig.4a). After chemical activation using HCl (AM-2C, Fig. 4c) followed by plasma-deposition of FeOOH without ageing (AM-FeOOH-30/0C, Fig. 4d), isotherms are of type IV, characteristic of mesoporous materials, with the shapes of hysteresis loop suggesting the presence of ink-bottle shape pores. The material resulting from activation of VA and deposition of FeOOH simultaneously by glidarc plasma, also shows isotherm type IV, characteristic of mesoporous material (Fig. 4b). This result proves that the simultaneous plasma-activation of VA and -deposition of FeOOH slightly improve the VA texture. The plasma-deposition of FeOOH on chemical activated VA, followed by ageing (AM-FeOOH-30/4C), does not induce any shift of the hysteresis loop (Fig. 4e), thus proves that the ageing does not significantly influence the mesoporosity or pore volume (Table 1). These results are contrary to those obtained by *Boyom et al. (2021)* who

reported that the ageing of MnO_2 at 100°C leads to a shift in the hysteresis loop towards higher pressures, suggesting the progressive evolution of mesoporosity towards macroporosity [26]. The chemical activation of VA using HCl leads to a decrease of pore diameter, indicating a gradual evolution from a weakly porous material to a highly mesoporous one (Table 1). The pore distribution curves of particles (Fig. 5) show an intense peak around 34 Å (a monomodal distribution) for materials resulting from the chemical activation of VA (AM-2C), plasma-deposition of FeOOH (AM-FeOOH-30/0C), and ageing (AM-FeOOH-30/4C), compared to VA and VA-FeOOH-30/0 materials which are non or weakly porous and for which no peak appears. This value falls within the range of mesoporous materials and approaches microporosity as shown in Fig. 5 and Table 1. After simultaneous plasma-activation of VA and -deposition of FeOOH (VA-FeOOH-30/0), the isotherm type IV remains unchanged with a more narrowed hysteresis, suggesting a very weak mesoporosity with non-uniform slit-like pores. This result more attests the previous statements made (FT-IR and XRD analyses) that simultaneous plasma-activation of raw VA and -deposition of FeOOH (VA-FeOOH-30/0) do not change its microstructure. Table 1 shows a decrease of the pore diameter, an increase of the specific surface area, and pores volume of VA after chemical activation using HCl (AM-2C) followed by ageing of plasma-deposition of FeOOH. Therefore, the dissolution of basic oxides and impurities contained within the VA by HCl generates cavities within its matrix, and plasma post-discharge species developing more active sites during the ageing. However, we observe that plasma-deposition of FeOOH on chemical activated VA without ageing induces a slight pores obstruction, explaining a slight decrease of the specific surface area. Nevertheless, we recorded a significant increase of the specific surface area of the plasma-deposited FeOOH after ageing, which could be ascribed to the maturation of the FeOOH deposited within the pores of AM-2C. Therefore, this result highlights a huge crystallite's nucleation thanks to plasma post-discharge species (H_2O_2 and HNO_3) related to the high microstructure change when using HCl as activating agent [1]. Otherwise, simultaneous plasma-activation of VA and -deposition of FeOOH (VA-FeOOH-30/0) lead to a slight increase of the specific surface area, suggesting that HNO_x species, electron-bombardment, and electroshock waves plasma-generated do not allow a better activation (microstructure modification) of VA when performing it simultaneously with deposition. This low value of VA-FeOOH-30/0 (25 m^2/g) compared to those derived from VA activated by HCl, proves that the chemical activation enhances the textural properties of VA for a good deposition of FeOOH by glidarc plasma.

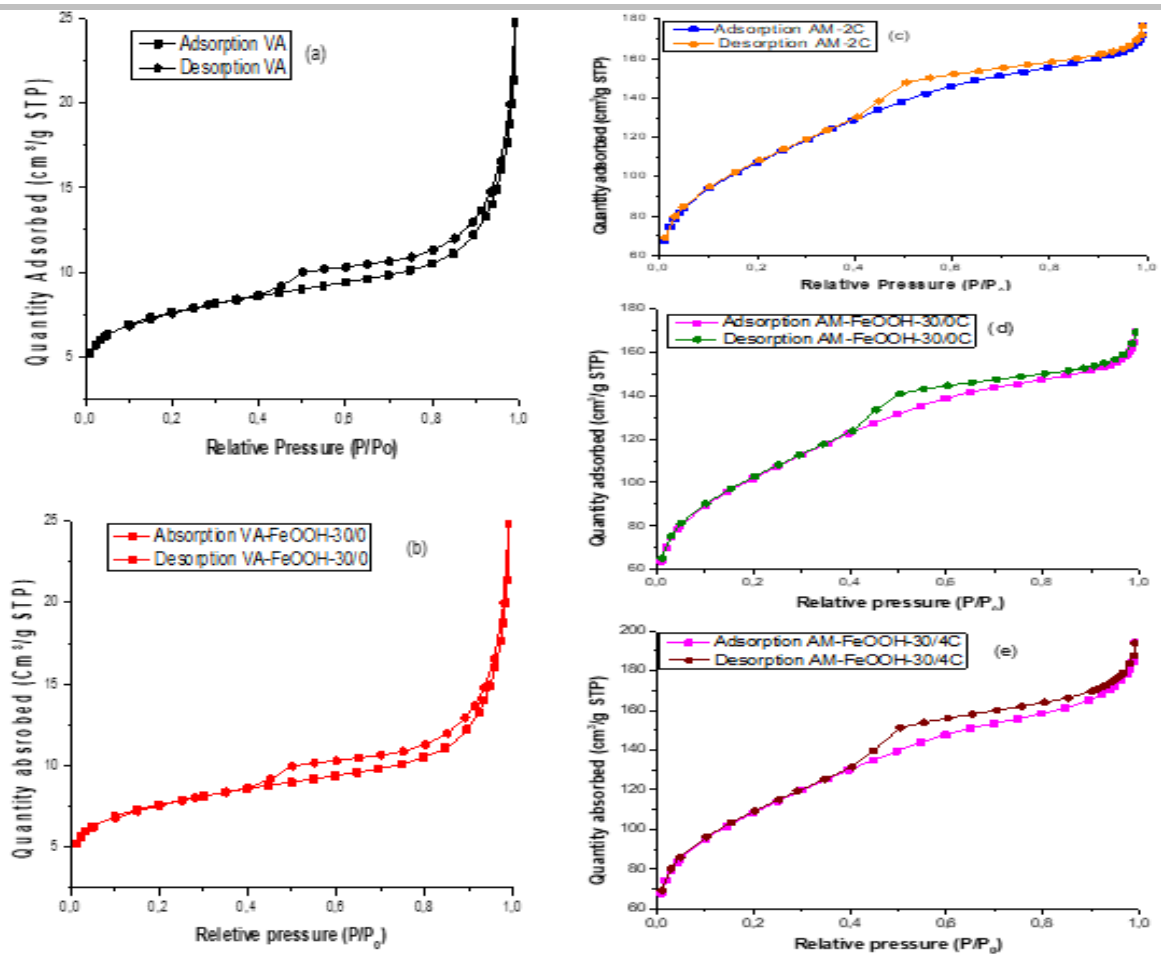

Figure 4. Adsorption and desorption isotherm of (a) Raw VA, (b) simultaneous plasma activated VA and deposited FeOOH (VA-FeOOH-30/0), (c)Activated AM-2C, (d) Chemical activated VA and plasma deposited FeOOH (AM-FeOOH-30/0C) and (e) Aged AM-FeOOH-30/4C materials.

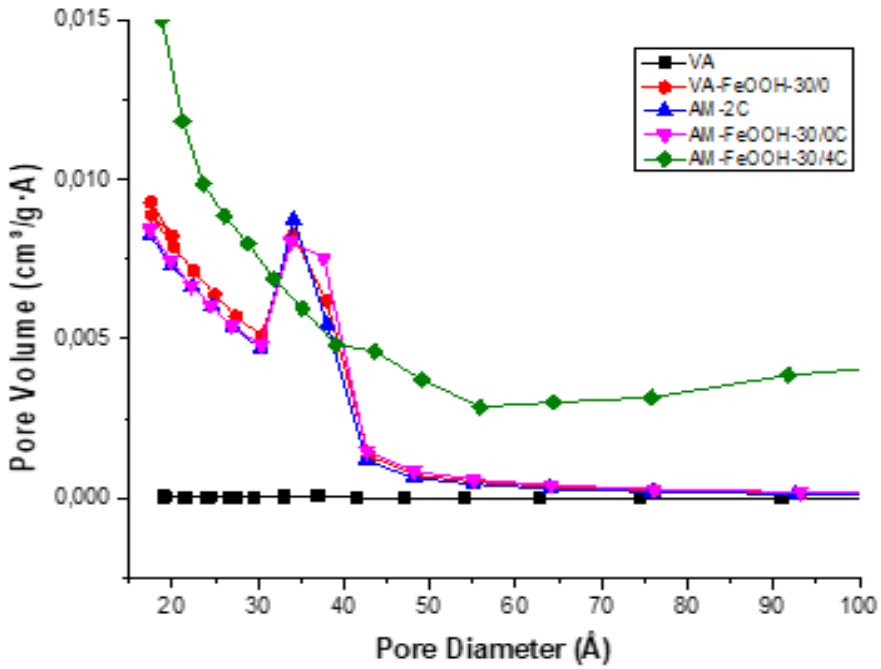

Figure 5. Pore distribution curve of: Raw VA, activated (AM-2C), simultaneous plasma activated VA and deposited FeOOH (VA-FeOOH-30/0), chemical activated VA and plasma deposited FeOOH (AM-FeOOH-30/0C) and Aged AM-FeOOH-30/4C materials.

Table 1. Textural data of different materials

Samples	S_{BET} (m^2/g)	Micro-porous Volume (cm^3/g)	Pore Volume (cm^3/g)	D_{BJH} (Å)
VA	3	0.000	0.010	81
VA-FeOOH-30/0	25	0.005	0.030	50
AM-2C	365	0.130	0.260	29
AM-FeOOH-30/0C	347	0.130	0.250	28
AM-FeOOH-30/4C	368	0.130	0.280	30

Scanning Electron Microscope (SEM) and Energy dispersive X-ray (EDX) analyses

We can see from the Fig. 6 that large agglomerates particles of VA material (Fig. 6a) become smaller after chemical activation using HCl (Fig. 6c) which corroborates the increase of the specific surface area recorded (Table 1). The chemical activated AM-2C material (Fig. 6c) appears as a collection of plates with fewer agglomerates compared to the raw material (Fig. 6a). We recorded almost the same changes as in our previous work, after using H_2SO_4 to chemically activate VA [1]. The plasma-deposited FeOOH on activated VA using HCl (Fig. 6d) shows slight fine edges on the surface indicating the addition of fine FeOOH particles (AM-FeOOH-30/0C). Furthermore, the VA-FeOOH-30/0 material resulting from the simultaneous plasma-activation of VA and -deposition of FeOOH (Fig. 6b) has a granular appearance and a less fine surface compared to AM-FeOOH-30/0C material, which has a better surface fineness with a more homogeneous distribution of FeOOH. The SEM images of AM-FeOOH-30/4C material resulting from the ageing of deposited FeOOH at 100°C for 4 hours, show a fine surface with smaller particle size and slit pores (Fig. 6e).

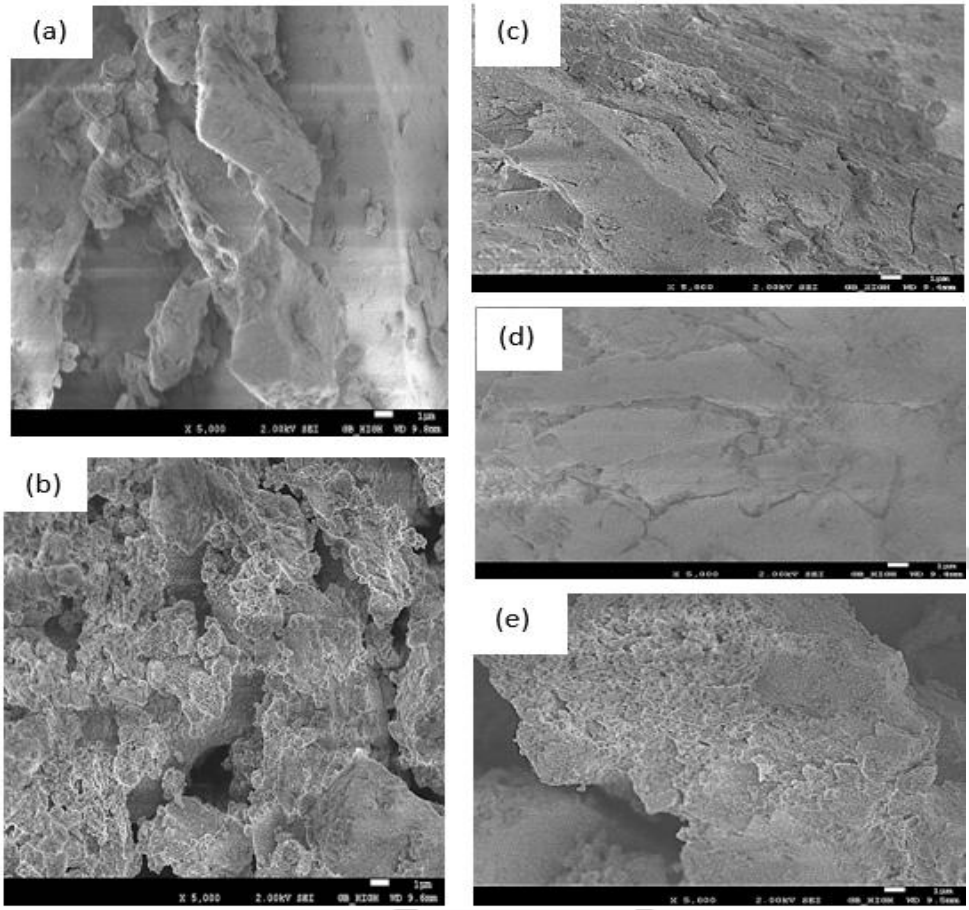

Figure 6. Micrographs (x5000) of (a) Raw VA, (b) simultaneous plasma activated VA and deposited **FeOOH** (VA-**FeOOH**-30/0), (c)Activated AM-2C, (d) Chemical activated VA and plasma deposited **FeOOH** (AM-**FeOOH**-30/0C) and (e) Aged AM-**FeOOH**-30/4C materials.

Table 2 summarizes the surface elemental composition of the different materials. The raw material (VA) is mainly composed of oxygen, silicon, aluminum, and iron, while as minor elements it contains calcium, magnesium, phosphorus, titanium, and sodium, all with an heterogeneous distribution on the surface (Fig. S_3). The chemical activation of VA using HCl leads to an increase in the Si/Al ratio (13.5), and a decrease in the Fe/O ratio (Table 2), respectively attributed to the dealumination and the dissolution of oxidized iron fractions by HCl, thus explaining the increase of the specific surface area (Table 1). Therefore, activation using HCl results in hydrolytic rupture of the Si-O-T bonds (T=Al, Si, or Fe, Eq. 3) and condensation of Si-OH into Si-O-Si, forming mesoporous silica aggregates. The Si/Al ratio of the AM-2C material resulting from the action of HCl remains lower than that of the AM-2 material from H_2SO_4 [1], indicating that the activation of VA using HCl leads to the formation of a shorter condensation chain (during geopolymerization) than when performed with H_2SO_4. The plasma-deposition of FeOOH induces a decrease in the Si/Al ratio (11.6) with an increase of Fe/O ratio (0.06), which is contrary to what is observed during the chemical activation process. This decrease can be explained by a break in the surface bonds of AM-2C material, which induces a reorganization of the amorphous 3D aluminosilicate network. This can also be explained by the substitution of Si^{4+} by Al^{3+} with a charge deficit within the SiO_4^{4-} tetrahedra, whose compensation is ensured by extra-framework cations and exchanged ion. While a slight increase in the Fe/O ratio (from 0.005 to 0.06) after the plasma-deposition of FeOOH on the activated material (AM-2C) proves that the deposit increases proportionally with the grafting of plasma-generated HO groups on the surface. The aged material (AM-FeOOH-30/0C) reveals an increase in the Fe/O ratio (0.15) and confirms the aforementioned statements,

indicating that ageing (plasma post-discharge reactions) would lead to the maturation (nucleation evolution) of FeOOH crystallites and could explain the formation of α-Fe-O-OH on the material surface thanks to long-lived species such as H_2O_2 and HNO_2. The decreasing quantity of the Mg, Na, K, and Ca elements from 14.8% (VA) to 7.5% (VA-FeOOH-30/0) demonstrates that the basic oxides present reacted with the plasma-generated acid species HNO_3 and HNO_2. An increase in the Fe/O ratio after simultaneous plasma-activation of VA and -deposition of FeOOH (VA-FeOOH-30/0) from 0.3 to 0.8 proves that FeOOH particles have precipitated on the surface after plasma-activation. Studies conducted by *Hanon and Gaigneaux (2024)* show that in addition to HO• radicals, the long-lived species such as HNO_3 and HNO_2 would be responsible for the precipitation of Fe^{2+} and Fe^{3+} ions to FeOOH [27]. The decrease in the Si/Al ratio from 2.5 for VA to 0.2 for VA-FeOOH-30/0 material highlights an absence of polycondensation within the material. This further confirms that the activation of raw VA and deposition of FeOOH simultaneously by plasma do not sufficiently influence the porosity, as *Duxson et al. (2007)* showed that an increase in the Si/Al ratio would lead to a reduction of macropores into smaller pores [40]. The significant content of sulfur recorded after simultaneous plasma-activation of VA and -deposition of FeOOH could lead to the formation of calcium sulfate obstructing the pores, thus more explaining the weak specific surface area of VA-FeOOH-30/0 catalyst (Table 1). Therefore, VA could react with the precursor (heptahydrated iron sulfate) to form $[Fe(OH)_2]_2SO_4$, which has not been revealed by X-ray analysis, likely due to the low amount of sulfate ions compared to water in the medium. The same observation was made by *Hanon et al. (2024)* during the Glidarc plasma synthesis of mixed oxides using the precursor $(NH_4)_2Fe(SO_4)_2.6H_2O$ [27]. On the other hand, the low specific surface area of VA-FeOOH-30/0 material could be explained by the low dissolution of the basic oxides by nitrous and nitrite acids produced in Glidarc plasma medium.

$$[Si\text{-}O\text{-}Al]^{5+} + HCl + 7H_2O \rightarrow Si(OH)_4 + Al(OH)_4^- + Cl^- + 7H^+ \quad (3)$$

Table 2. Elemental composition on the surface of different materials

Elements	Samples (Mass %)				
	VA	VA-FeOOH-30/0	AM-2C	AM-FeOOH-30/0C	AM-FeOOH-30/4C
O	48	43	63.9	65.8	59.3
Si	14.8	0.8	28.3	23.2	26.5
Fe	14.1	32.7	0.3	3.9	9.1
Ca	6.5	3.9	1.7	2.4	1
Al	6.0	4.1	2.1	2	1.5
Mg	5.6	1.7	0.5	0.5	0.2
Na	1.7	1.1	0.5	0.3	0.2
K	1.1	0.7	0	0	0
S	0	1.5	0	0	0.6
P	0	-	0.6	0.5	0.2
Ti	1.9	1.5	-	-	-
Si/Al	2.5	0.2	13.5	11.6	17.7
Fe/O	0.3	0.8	~0.0	0.1	0.2

Determination of pH at the point of zero charge

The surface charge of different materials has been determined to evaluate the interactions that may occur during the catalytic degradation process of the pollutant (Rh-6G) at the catalyst surface. Fig. 7 depicts the point of zero charge (pH_{PZC}) of different materials. The results show a progressive decrease in pH_{PZC} after chemical activation of VA using HCl (AM-2C), plasma-deposition of FeOOH without ageing (AM-FeOOH-30/0C), and ageing of the deposited material in boiling water bath (AM-FeOOH-30/4C). This can be explained by the fact that chemical activation of VA using HCl leads to the grafting of protons H^+ on the surface, thus lowering the pH_{PZC}. The plasma through its acidic properties [42], further binds H^+ protons at the surface of VA, resulting in a pH_{PZC} decrease. Otherwise, the chemical activation of the VA using HCl significantly increases the acidity order of the materials (AM-2C, AM-FeOOH-30/0C and AM-FeOOH-30/4C) compared to what was recorded after using H_2SO_4 in our previous work [1]. This deeply highlights a more marked VA microstructure's change when chemical activation is performed using HCl as previously mentioned. Moreover, the pH_{PZC} decrease can also be attributed to the insertion of Fe^{2+} and Fe^{3+} into the cavities of activated VA in the form of Lewis acid sites. Therefore, these recorded pH_{PZC} values indicate that, under the optimal conditions for catalytic degradation of Rhodamine-6G (pH=7), the surface of all materials except for the raw VA material (pH_{PZC}=8.0) is negatively charged, thus promoting an electrostatic attraction with the positive charges of the pollutant molecules. The plasma-deposited (AM-FeOOH-30/0C), and aged (AM-FeOOH-30/4C) materials show lower pH_{PZC} values than that obtained from the simultaneous plasma-activation of VA and -deposition of FeOOH (4.8). This suggests that plasma-deposited (supported) and aged

materials have many more acidic sites on their surface, and will have a greater affinity for the pollutant molecules and may lead to a strong adsorption, thus a better degradation rate of the pollutant. At pH lower than the zero charge point of the different materials, their surfaces are positively charged which could induce an electrostatic repulsion between the surface of each material and the positive charges of the cationic pollutant molecules [1]. Furthermore, the decrease in pH_{PZC} from 8.0 for VA to 4.7 for VA-FeOOH-30/0 shows that, thanks to the acidifying properties of plasma, activation of raw VA is possible.

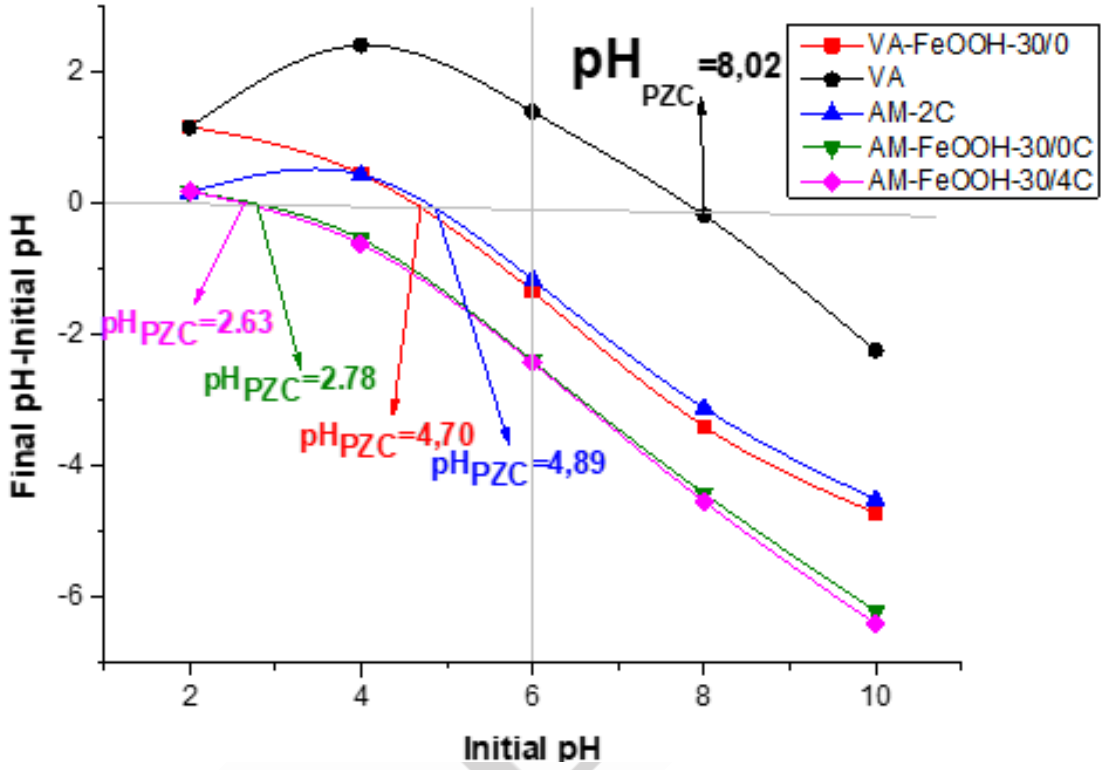

Figure 7. Point zero charge of Raw (VA), Activated (AM-2C), simultaneous plasma activated VA and deposited FeOOH (VA-FeOOH-30/0), Chemical activated VA and plasma deposited FeOOH (AM-FeOOH-30/0C) and Aged AM-FeOOH-30/4C materials.

3.2. Fenton catalytic tests of different materials

Fig.8 shows the evolution of the UV-Vis spectrum of Rhodamine-6G (25 mg/L) after Fenton catalytic treatment with different materials as catalysts. We can see two distinct bands: the first in the UV region (λmax = 347 nm) and the second in the visible region with an overlay of two signals around 480-490 nm and a maximum absorption (λmax) around 513 nm, corresponding to π-π* (C=C) and n-π* (-HN-C et O=C) transitions of the Rhodamine-6G molecule responsible for its color. The spectra resulting from the degradation of Rhodamine-6G using AM-2C, AM-FeOOH-30/0C, and AM-FeOOH-30/4C materials, show a significant decrease of both absorption bands, describing the destruction of the chromophore groups and aromatic cycle of Rhodamine-6G. The hypochromic shift around these two absorption bands after treatment with the different materials indicates the degradation of Rhodamine-6G via the rupture of the conjugated chromophore groups occurring at the maximum wavelength of 513 nm [43]. The use of chemical activated (AM-2C), plasma-deposited (AM-FeOOH-30/0C), and aged (AM-FeOOH-30/4C) materials shows a remarkable decrease in absorption intensity, which can be explained by the accessibility and reactivity of the sites present at the catalyst surface, as induced by the chemical activation of VA using HCl. This result corroborates the findings of *Ghazzal et al. (2012),* who reported that pronounced porosity induces a better adsorption of the Rhodamine-6G monomer [44]. AM-2C material resulting from the

chemical activation of VA without FeOOH deposition exhibited a higher degradation rate. This could be explained by the facts that the large pores developed at the VA surface's (specific surface area, Table 1) promote a large adsorption of the pollutant molecules, and that a non-negligible catalytic process occurs between the remaining iron at the AM-2C surface (Table 2) and H_2O_2, generating reactive oxidizing species such as hydroxyl radicals (HO•).

Moreover, VA-FeOOH-30/0 material resulting from the simultaneous plasma-activation of VA and -deposition of FeOOH weakly degrades Rhodamine-6G , which corroborates the unchanged microstructure of raw VA and its weak specific surface area (Table 1). Knowing that Fenton's photodegradation is a surface phenomenon, the low specific surface area recorded (Table 1) can explain the low pollutant removal. This corroborates the work of *Hanna et al. (2008)*, who showed that the degradation rate of methylene blue decreased as the specific surface area of the mixed iron and silica oxides also decreased [45]. Even if the pore diameter of the VA-FeOOH-30/0 (50Å) is larger than those of AM-FeOOH-30/0C (28Å) and AM-FeOOH-30/4C (30Å) materials, a low degradation rate of Rh-6G is observed. Thus, the low degradation of Rh-6G using VA-FeOOH-30/0 material could also be attributed to its non (or very weak) porous nature inducing its weak activity compared to AM-FeOOH-30/0 (plasma-deposited) and AM-FeOOH-30/0C (aged) materials.

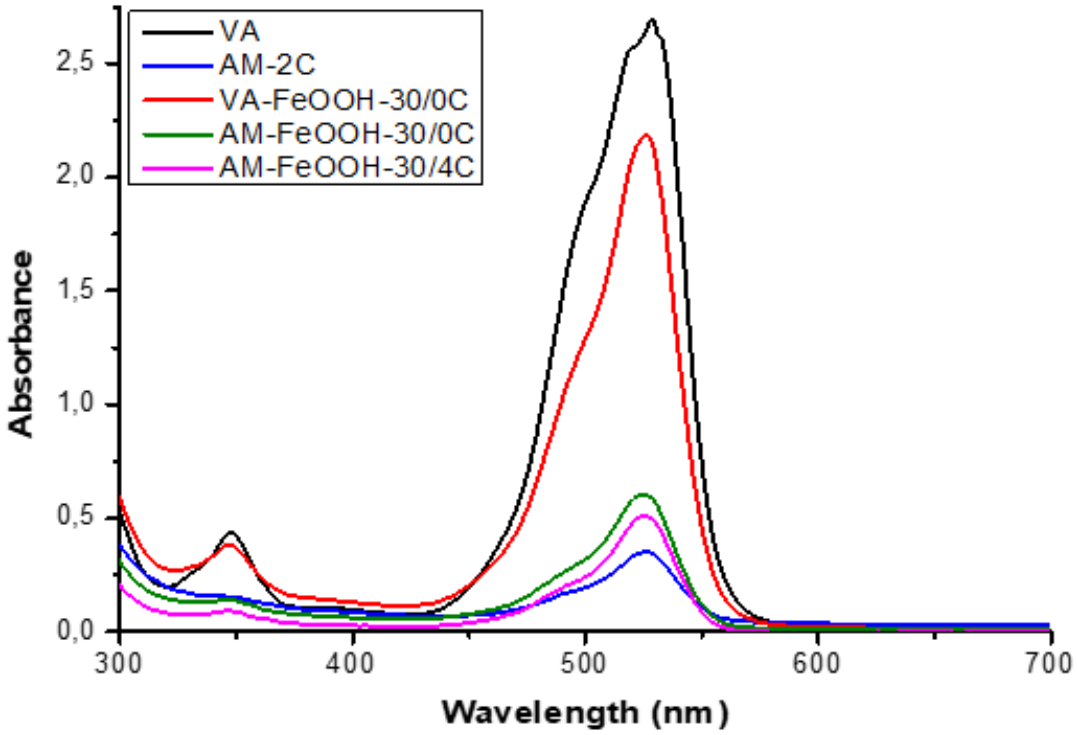

Figure 8. Evolution of UV-Vis spectrum of Rh-6G after catalytic treatment with daylight (pH=7, t=20 min, [Rh-6G] = 25mg/L, [Catalyst]=3g/L, 1ml of H_2O_2).

Evaluation of post-catalytic treatment of Rhodamine 6G

The evolution of the pollutant degradation rate after the removal of the catalyst from the reaction medium was performed in the dark, and the results obtained are depicted in Fig. 9. As shown on Fig.9a, *in situ* catalytic treatment of Rh-6G (25 mg/L) gave after 20 min degradation rates of 31, 32, 87, 78, 82% respectively with VA, VA-FeOOH-30/0, AM-2C, AM-FeOOH-30/0C and AM-FeOOH-30/4C. Therefore, our plasma-deposited FeOOH on chemical activated VA appears more effective than Biochar/Bi_2WO_6 catalyst prepared via hydrothermal route which

revealed 99.9% after 250 min of the visible photo-degradation of Rhodamine B (10 mg/L) [46]. However, a notable degradation rate is observed after the removal of each catalyst in the reaction medium (post-catalytic exposure). We observe a significant increase of the Rh-6G degradation rate after 24 and 48 hours of post-catalytic Fenton treatment (Fig.9b), compared to *in situ* catalytic Fenton treatment for 20 minutes (Fig. 9a). This highlights the degradation process of Rh-6G molecule thanks to the oxidizing species produced *in situ* during the catalytic Fenton process in daylight. The electrons (e^-) from conduction band and generated holes (h^+) in the valence band respectively react with dissolved oxygen and water molecules, to form powerful oxidizing species ($HO^{\bullet}$, H_2O_2, $O_2^{-\bullet}$) capable of effectively mineralizing Rh-6G molecules [1]. In addition, the oxidizing species HO• formed *in situ* through the decomposition of hydrogen peroxide by each catalyst (Fenton-like reactions) recombine to reform large quantities of oxidizing species such as hydrogen peroxide (a long-lived species), leading to the degradation of Rhodamine-6G during the post-treatment in the dark. This result attests the fact that in addition to the adsorption of Rh-6G on the catalyst's surface, the degradation process of the pollutant molecule really occurs.

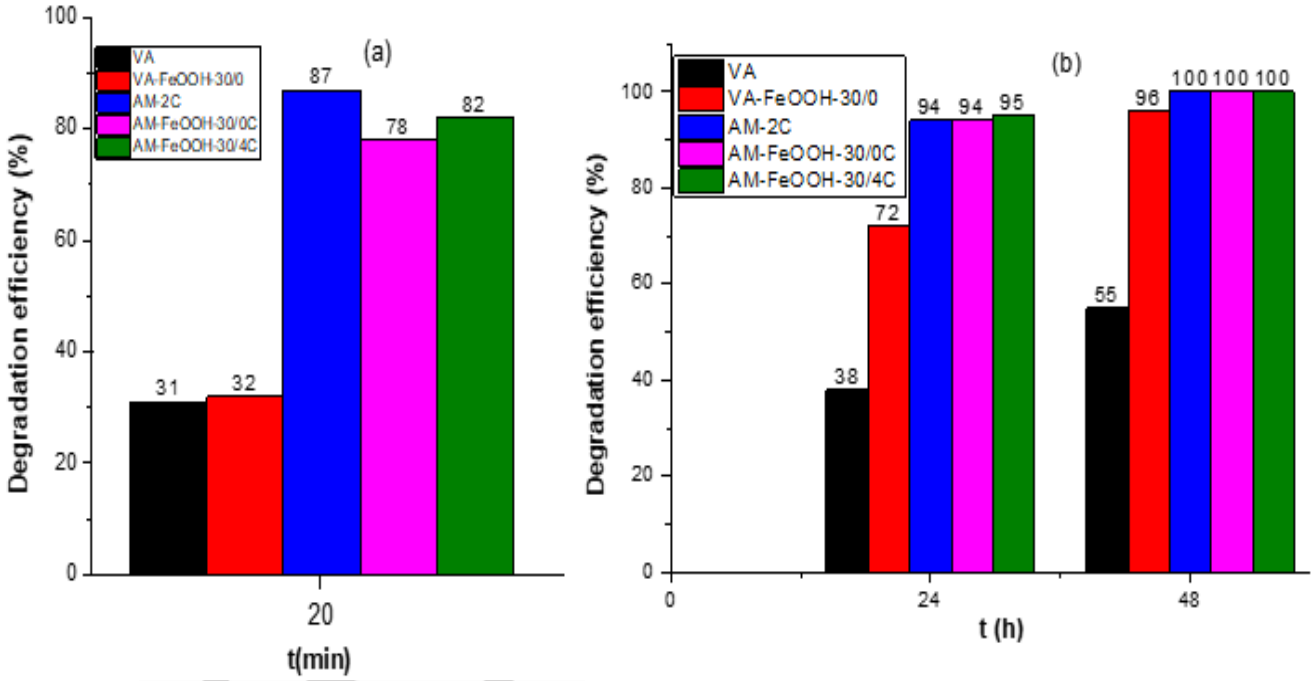

Figure 9. (a) In situ catalytic and (b) post-catalytic treatment of Rhodamine 6G using VA; AM-2C; AM-FeOOH-30/0C; AM-FeOOH-30/4C; VA-FeOOH-30/0) materials, (t=20 min, 3g/L, pH=7, [Rh-6G] =25 mg/L).

Catalytic stability and leaching test

Knowing that catalytic stability is one of the requirements for a good industrial application of catalysts, we assessed our prepared materials during four successive catalytic cycles (Fig. 10). Despite a slight efficiency decrease of the chemical activated material (AM-2C), those resulting from the plasma-deposition without ageing (AM-FeOOH-30/0C) and ageing (AM-FeOOH-30/4C) revealed a very high catalytic stability during their reuse and corroborate their leaching test (Table 3) which did not show any iron leached after four catalytic cycles. In our previous work, the use of the material resulting from the activation of VA using H_2SO_4 revealed a decreasing degradation rate of Rhodamine-6G during catalytic oxidation, due to the leaching of iron and the potential clogging of the pores due to the formation of calcium sulfate [1], which is not the case in the present work. Otherwise, the gradual decrease of the catalytic efficiency of AM-2C material could be explained by the progressive occupation/obstruction of the adsorption sites by the pollutant molecule during the successive catalytic cycles. VA-

FeOOH-30/0 material resulting from the simultaneous plasma-activation and -deposition of FeOOH shows a significant increase of the degradation degree during the four cycles, compared to AM-FeOOH-30/0C material resulting from chemical activated VA followed by plasma-deposition of FeOOH whose activity remains stable. *Zhu et al. (2025)* also reported a catalytic stability of the nanocomposites based on Iron, Nickel and Molybdate prepared via hydrothermal route, after the fifth Fenton catalytic degradation cycle of Rhodamine B [47]. The behavior of VA-FeOOH-30/0 material could be explained by the progressive leaching of active phase (FeOOH) during the four catalytic cycles, thereby increasing the degradation efficiency (homogeneous Fenton catalysis) of the catalyst despite its dissolution (Table 3). The VA-FeOOH-30/0 material thus shows a greater structural instability compared to the plasma-deposited (AM-FeOOH-30/0C) and aged (AM-FeOOH-30/4C) materials which remain stable. Therefore, the low degradation rate of Rhodamine-6G using VA-FeOOH-30/0 material can be attributed to the trapping of HO• radicals by the excess iron on the material surface. This proves that the progressive leaching of iron from VA-FeOOH-30/0 material during the four catalytic cycles (Table 3) could induce homogeneous Fenton catalysis through reaction with hydrogen peroxide in the medium, explaining the increase of the degradation rate after each cycle (Fig.10). Therefore, simultaneous plasma-activation of VA and -deposition of FeOOH (VA-FeOOH-30/0) do not allow a better catalytic stability of the corresponding material during the degradation of Rhodamine-6G compared to those resulting from the plasma-deposition of FeOOH on chemically activated VA (AM-FeOOH-30/0C).

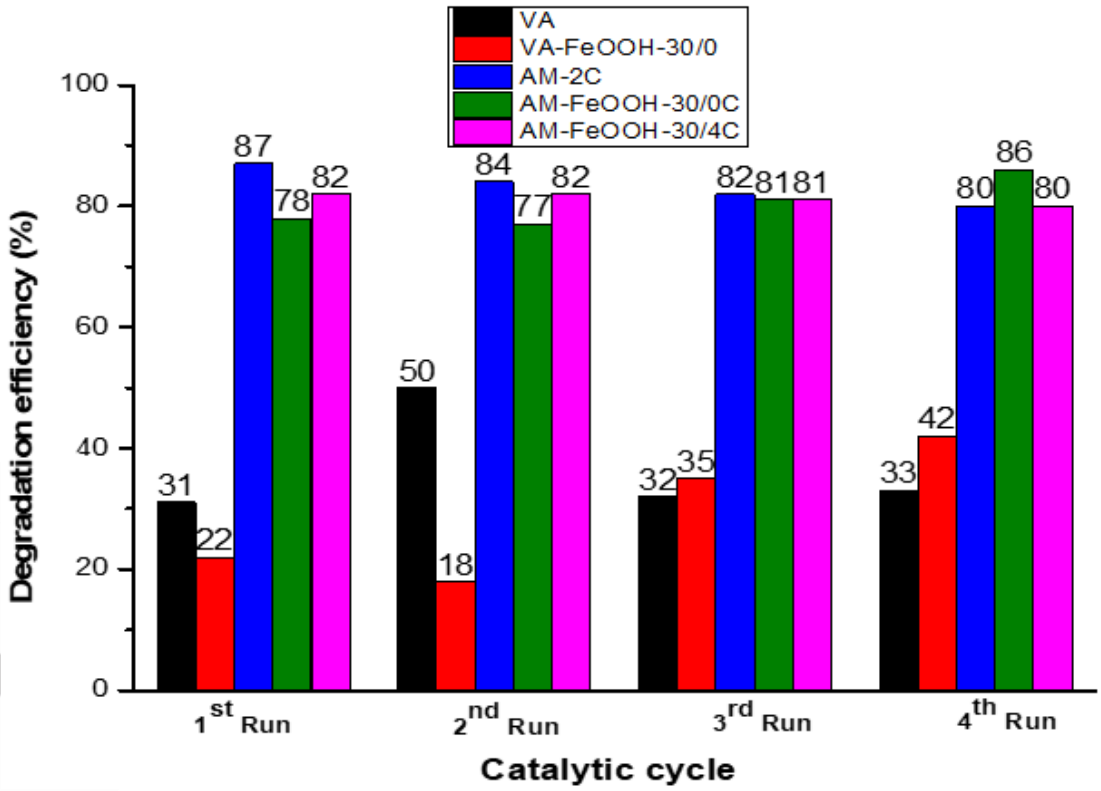

Figure 10. Catalytic reuse of different materials (pH=7, [Catalyst]=3g/L, t=20 min, [Rh-6G] =25 mg/L).

Table 3. Iron leaching tests during different catalytic cycles of different materials

	Leached iron (mmol. L^{-1})			
Cycle	1	2	3	4
VA	0.0030	0.0020	0.0005	0
VA-FeOOH-30/0	0.0001	0.0004	0.0026	0.0089
AM-2C	0	0	0	0
AM-FeOOH-30/0C	0	0	0	0
AM-FeOOH-30/4C	0	0	0	0

Fig.11 shows the XRD patterns (Fig. 11a) and FTIR spectra (Fig.11b) of VA-FeOOH-30/0 and AM-FeOOH-30/0C materials before and after the first catalytic cycle (use). Fig.11a shows that the material obtained via chemical activation of the VA followed by the plasma-deposition of FeOOH (AM-FeOOH-30/0C) does not show any significant structural change after catalytic use (AM-FeOOH-30/0C-used). However, VA-FeOOH-30/0 material from simultaneous plasma-activation of VA and -deposition of FeOOH reveals a change of its crystalline structure after catalytic use (VA-FeOOH-30/0-used) through the formation of new amorphous phase. This result highlights a better plasma-deposition of FeOOH on the chemical activated VA (AM-FeOOH-30/0C) leading to its catalytic stability during four cycles, than simultaneous plasma-activation and -deposition route (VA-FeOOH-30/0-used), of which the obtained material leached (Table 3) and generated the amorphous phases. The FTIR spectrum of VA-FeOOH-30/0-used (Fig.11b) does not show any new adsorption band, but rather a decrease of the absorption bands width around 1048 and 3346 cm^{-1}, which could be explained by the formation of the amorphous phase within the material as previously revealed by XRD analysis. The disappearance of the band around 694 cm^{-1} indicates the breaking of the Si-O-Al bond and confirms the structural modification of VA-FeOOH-30/0 material after use. For AM-FeOOH-30/0C material, the bands shift to higher wavenumbers (from 1048 to 1066 cm^{-1}) and the appearance of new band around 610 cm^{-1} indicate the formation of Si-O-Si bonds within the material after use (AM-FeOOH-30/0-used). The band around 793 cm^{-1} remains unchanged and confirms the presence of the active phase (FeOOH) within the material after use and corroborates the non-leaching previously recorded (Table 3). These results agree with XRD analysis, which demonstrate a reorganization of the material's structure while still showing the existence of the active phase (FeOOH) embedded in the amorphous aluminosilicate phase, thus highlighting the better plasma-deposition on the chemically-activated VA.

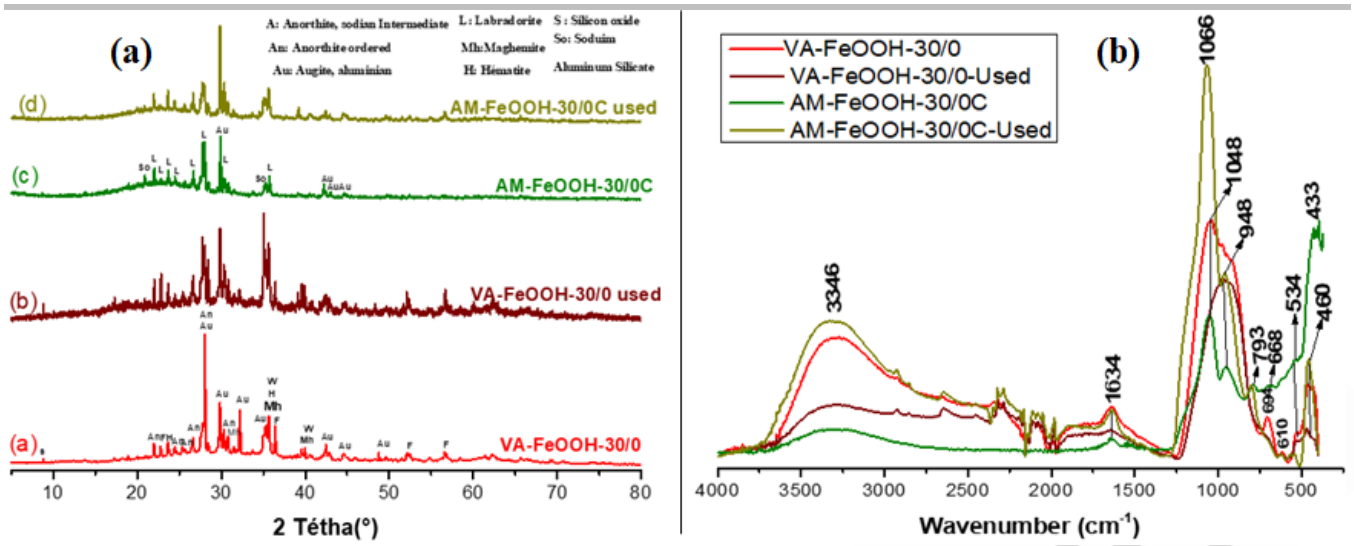

Figure 11. Physicochemical characterization of the catalyst before and after use: (a) XDR and (b) FTIR analysis: (VA-FeOOH-30/0) activated VA and deposited FeOOH simultaneous by plasma, (AM-FeOOH-30/0C) Chemical activated VA and plasma-deposited FeOOH by plasma.

Conclusion

Chemical activation of the volcanic ash (VA) as support using HCl solution followed by plasma-deposition of FeOOH particles was compared to simultaneous plasma-activation of VA and -deposition of FeOOH. The use of HCl as an activating agent of VA, largely modifies the microstructure, improves the texture (specific surface area and porosity) of the VA, and limits the formation of calcium sulphate when H_2SO_4 is used (previous work), which could induce pores obstruction. Therefore, using HCl solution to activate VA allows a better plasma-deposition of FeOOH (AM-FeOOH-30/0C). Moreover, plasma post-discharge species such as H_2O_2 and HNO_3 induce the evolution of the crystallite's nucleation, and thereby significantly improves the specific surface area and porosity of the obtained material (AM-FeOOH-30/4C). As a counterpart, performing the simultaneous plasma-activation of VA and -deposition of FeOOH did not induce a significant structure and texture modification of the obtained material (VA-FeOOH-30/0). Therefore, plasma conditions in the current work did not allow to carry out plasma-activation of VA and -deposition of FeOOH simultaneously. Materials resulting from, plasma deposited FeOOH on the chemical activated VA using HCl (AM-FeOOH-30/0C), and aged (AM-FeOOH-30/4C) exhibit stable catalytic activity with no iron dissolution. Compared to the two previous materials, the one obtained by simultaneous plasma-activation of VA and -deposition of FeOOH (VA-FeOOH-30/0) shows a low activity and huge dissolution/leaching of iron during catalytic tests, which could be ascribed to the weak activation of VA and FeOOH deposition. Thus, for a good dispersion and anchoring of the active phases (FeOOH) on VA, a chemical activation using HCl is necessary to obtain a good porous support with a large specific surface area, and stable catalytic activity/structure. This work promotes volcanic ash as a local material for an effective preparation of heterogeneous Fenton catalysts with better degradation efficiency of organic pollutants in aqueous solution. However, to better perform the simultaneous plasma-activation of the VA and the plasma-deposition of FeOOH particles, it would be interesting to increase the reactivity in plasma medium by exploring some parameters changes. On the other hand, we could also consider carrying out both processes separately.

Supporting Information

Physico-chemical properties of pollutant (Rhodamine-6G), scheme of gliding arc plasma with the *in situ* and post-discharges generated species, EDX, FTIR and N_2 physisorption data.

Acknowledgements

We also thank the MIPROMALO (Mission for the Promotion of Local Materials in Cameroon) for volcanic ash provided.

Declaration of Competing Interest

The authors declare that they have no known competing financial interests or personal relationships that could have appeared to influence the work reported in this paper.

Keywords: FeOOH supported catalysts • Volcanic ash • Glidarc Plasma-activation/deposition • Heterogeneous Fenton catalysis • Rhodamine-6G degradation

References

[1] M. Pitap-Mbowou, F. W. Boyom-Tatchemo, E. Acayanka, G. Kamgang-Youbi, C. Poupin, S. A. Gámez-Rivera, R. Cousin, E. M. Gaigneaux, S. Laminsi, Activation of volcanic ash as support for FeOx gliding arc plasma deposition and application in the catalytic oxidation of Rhodamine 6G, J. Environ. Chem. Engi. ***2024***,*12:6,* 11589. https://doi.org/10.1016/j.jece.2024.114589.

[2] N. Miloh, V. K. Kengne, E. Acayanka, P. M. Kouotou, G. Kamgang-Youbi, Plasma-assisted Synthesis of Supported Superparamagnetic Oxides for Enhanced Fenton Reactions, Water. Air. Soil. Pollut. ***2024***, *235:10*, 631. https://doi.org/10.1007/s11270-024-07446-1.

[3] U. U. Ashar, M. Anis, G. Hussain, A. Tauseef, Hybrid treatment of textile wastewater through catalytic thermolysis and catalytic heterogeneous Fenton processes, Int. J. Environ. Sci. Technol**. *2025***, *22:2,* 1029-1042. https://doi.org/10.1007/s13762-024-05695-5.

[4] N. Demir, G. Gündüz, M. Dükkancı, Degradation of a textile dye, Rhodamine 6G (Rh6G), by heterogeneous sonophotoFenton process in the presence of Fe-containing TiO_2 catalysts, Environ. Sci. Pollut. Res. ***2015***, *22,* 3193-3201. https://doi.org/10.1007/s11356-014-2868-x.

[5] S. Papić, D. Vujević, N. Koprivanac, D. Šinko Decolourization and mineralization of commercial reactive dyes by using homogeneous and heterogeneous Fenton and UV/Fenton processes, J. Hazard. Mater. ***2009***, *164:2-3,* 1137-1145. https://doi.org/10.1016/j.jhazmat.2008.09.008 .

[6] A. Tiya-Djowe, P. N. Lemougna, A. Emadak, M. Pitap-Mbowou, S. Laminsi, U. C. Melo, Taking advantage of iron contained in natural volcanic ash for catalytic degradation of Rhodamine 6G, Surf. Interfaces. ***2018***, Issn. 3:1-3. https://doi.org/10.48442/IMIST.PRSM/jasi-v3i1-3.11169.

[7] A. N. Soon, B. H. Hameed, Heterogeneous catalytic treatment of synthetic dyes in aqueous media using Fenton and photo-assisted Fenton process, Desalination. ***2011***, *269:1-3*, 1-16. https://doi.org/10.1016/j.desal.2010.11.002.

[8] P. H. Sreeja, K. J. Sosamony, A comparative study of homogeneous and heterogeneous photo-Fenton process for textile wastewater treatment, Proc. Technol. ***2016***, *24,* 217-223. https://doi.org/10.1016/j.protcy.2016.05.065.

[9] J. Chen, L. Zhu, Heterogeneous UV-Fenton catalytic degradation of dyestuff in water with hydroxyl-Fe pillared bentonite, Catal. Today. ***2007***, *126:3-4*, 463-470. https://doi.org/10.1016/j.cattod.2007.06.022.

[10] A. Styskalik, D. Skoda, C. E. Barnes, Pinkas, J. The power of non-hydrolytic sol-gel chemistry: Rev. Catal. ***2017***, *7:6*, 168. https://doi.org/10.3390/catal7060168.

[11] A. Tiya-Djowe, E. Acayanka, A. P. Mbouopda, F. W. Boyom-Tatchemo, S. Laminsi, E. M. Gaigneaux, Producing oxide catalysts by exploiting the chemistry of gliding arc atmospheric plasma in humid air. Catal Today. ***2019***, *334*, 104-112. https://doi.org/10.1016/j.cattod.2019.01.008.

[12] J. B. Tarkwa, E. Acayanka, B. Jiang, N. Oturan, G. Kamgang-Youbi, S. Laminsi, M. A. Oturan, Highly efficient degradation of azo dye Orange G using laterite soil as catalyst under irradiation of non-thermal plasma. Appl. Catal. B. ***2019***, *246,* 211-220. https://doi.org/10.1016/j.apcatb.2019.01.066.

[13] A. Tiya-Djowe, N. Ruth, G. Kamgang-Youbi, E. Acayanka, S. Laminsi, E. M. Gaigneaux, FeOx-kaolinite catalysts prepared via a plasma-assisted hydrolytic precipitation approach for Fenton-like reaction, Microporous. Mesoporous. Mater. ***2018***, *255,* 148-155. https://doi.org/10.1016/j.micromeso.2017.07.036.

[14] T. Meng, P. Xie, H. Qin, H. Liu, W. Hua, X. Li, Z. Ma Fe_2O_3/SiO_2 nanowires formed by hydrothermally transforming SiO_2 spheres in the presence of Fe^{3+}: Synthesis, characterization, and catalytic properties, J. Mol. Catal. A. Chem. ***2016***, *421,* 109-116. https://doi.org/10.1016/j.molcata.2016.05.017.

[15] M. S. Vasilyeva, V. S. Rudnev, A. A. Zvereva, A. Y. Ustinov, O. D. Arefieva, V. G. Kuryavyi, G. A. Zverev, FeOx, SiO_2, TiO_2/Ti composites prepared using plasma electrolytic oxidation as photo-Fenton-like catalysts for phenol degradation. J. Photochem. Photobiol. A. ***2018***, *356*, 38-45. https://doi.org/10.1016/j.jphotochem.2017.12.007.

[16] H. Hassan, B. H. Hameed, Fe–clay as effective heterogeneous Fenton catalyst for the decolorization of Reactive Blue 4, Chem. Eng. J. ***2011***, *171:3*, 912-918. https://doi.org/10.1016/j.cej.2011.04.040.

[17] H. Fida, G. Zhang, S. Guo, A. Naeem, Heterogeneous Fenton degradation of organic dyes in batch and fixed bed using La-Fe montmorillonite as catalyst, J. Colloid. Interface. Sc. ***2017***, *490,* 859-868. https://doi.org/10.1016/j.jcis.2016.11.085.

[18] H. Lim, J. Lee, S. Jin, J. Kim, J. Yoon, T. Hyeon, Highly active heterogeneous Fenton catalyst using iron oxide nanoparticles immobilized in alumina coated mesoporous silica. Chem. Commun. ***2006***, *4*, 463-465. DOI: 10.1039/b513517f.

[19] S. Bariyah, L. Simatupang, Activation of Sinabung Mount Volcanic Ash using Various Mineral Acids, Indones. J. Chem. Sci. Technol. ***2020***, *4:1*, 1-4. https://doi.org/10.24114/ijcst.v4i1.23087.

[20] F. Hanon, M. Devillers, E. M. Gaigneaux, Towards the Understanding of Parameters Allowing to Anticipate the Precipitation Reaction of Metallic Precursors in Humid Air Gliding Arc Plasma Reactor. Plasma Chem. Plasma. Process. ***2024***, 1-28, https://doi.org/10.1007/s11090-024-10516-1.

[21] F. Hanon, S. Hermans, E. M. Gaigneaux, What are the species involved in the gliding arc plasma synthesis of heterogeneous catalysts? Catal Today, ***2024***, *430*, 114550. https://doi.org/10.1016/j.cattod.2024.114550.

[22] G. Dionmbete, N. Miloh, J. B. Tarkwa, E. Acayanka, A. P. Mbouopda, F. W. Boyom-Tatchemo, G. Kamgang-Youbi, Hybrid composite with lignocellulosic biomass supported titania obtained under plasma conditions for photocatalytic application, Biomass. Convers. Biorefin. ***2023***, 1-15. https://doi.org/10.1007/s13399-023-04246-1.

[23] F. Hanon, E. M. Gaigneaux, Improving the synthesis of heterogeneous catalysts by gliding arc plasma using the “no-cooling system”, Appl. Mater. Today. ***2024***, *40*, 102408. https://doi.org/10.1016/j.apmt.2024.102408.

[24] C. F. Mbafou, B. Takam, F. W. Boyom-Tatchemo, J. B. Tarkwa, E. Acayanka, G. Kamgang-Youbi, S. Laminsi, Egg-derived porous plasma modified clay composite for wastewater remediation. Environ. Sci. Pollut. Res. ***2023***, *30:3*, 6612-6626. https://doi.org/10.1007/s11356-022-22617-5.

[25] B. Sop Tamo, G. Kamgang-Youbi, E. Acayanka, L. Medjo Simo, A. Tiya-Djowe, D. Kuete-Saa, L. Tchadjie, Plasma chemical functionalisation of a Cameroonian kaolinite clay for a greater hydrophilicity, Plasma. Chem. Plasma. Process. ***2016***, *36*, 1449-1469. https://doi.org/10.1007/s11090-016-9731-4.

[26] F. W. Boyom-Tatchemo, F. Devred, S. Laminsi, E. M. Gaigneaux, Temporal post-discharge reactions effect on the oxidative catalytic properties of plasma-synthesized α-MnO_2 nanorods, Appl. Catal. A. ***2021***, *616*, 118109. https://doi.org/10.1016/j.apcata.2021.118109.

[27] D. M. Chesseu, E. Acayanka, B. Takam, L. N. Line, G. Kamgang-Youbi, S. Laminsi, A. Bonilla-Petriciolet, Influence de la fonctionnalisation de surface à base de plasma des fibres de palmier sur l'adsorption du diclofénac de l'eau : expériences, thermodynamique et mécanisme d'élimination, J. Water. Chem. Technol. ***2021***, *43*, 102254 https://doi.org/10.1016/j.jwpe.2021.102254.

[28] A. Tiya-Djowe, S. Laminsi, G. L. Noupeyi, E. M. Gaigneaux, Non-thermal plasma synthesis of sea-urchin like α-FeOOH for the catalytic oxidation of Orange II in aqueous solution. Appl. Catal. B. ***2015***, *176*, 99-106. https://doi.org/10.1016/j.apcatb.2015.03.053.

[29] J. H. De Boer, B. C. Lippens, B. G. Linsen, J. C. P. Broekhoff, A. Van den Heuvel, T. J. Osinga, Thet-curve of multimolecular N_2-adsorption, J. Colloid. Interface. Sci. ***1966***, *21:4*, 405-414. https://doi.org/10.1016/0095-8522(66)90006-7.

[30] K. D. Belaid, S. Kacha, Étude cinétique et thermodynamique de l'adsorption d'un colorant basique sur la sciure de bois, Rev. Sci. Eau. ***2011***, *24:2*, 131-144. https://doi.org/10.7202/1006107ar.

[31] S. O. Otieno, F. O. Kengara, C. O. Kowenje, R. Mokaya, Hydrothermal synthesis of zeolites using silica extracted from tropical volcanic ash, Mater. Adv. ***2023***, *4:10*, 2292-2300. https://doi.org/10.1039/D3MA00065F.

[32] P. E. A. Lima, R. S. Angélica, R. F. Neves, Dissolution kinetics of metakaolin in sulfuric acid: comparison between heterogeneous and homogeneous reaction methods, Appl. Clay. Sci. ***2014***, *88*, 159-162. https://doi.org/10.1016/j.clay.2013.12.009.

[33] B. D. L. Ndjock, R. A. Robayo-Salazar, R. M. Gutiérrez, J. Baenla, J. A. Mbey, M. Cyr, A. Elimbi, Phosphoric acid activation of volcanic ashes: Influence of the molar ratio R=(MgO+ CaO)/P_2O_5 on reactivity of volcanic ash and strength of obtained cementitious material, J. Build. Eng. ***2021***, *33*, 101879. https://doi.org/10.1016/j.jobe.2020.101879.

[34] C. Belviso, M. Abdolrahimi, D. Peddis, E. Gagliano, M. Sgroi, A. Lettino, F. Cavalcante, Synthesis of zeolite from volcanic ash: Characterization and application for cesium removal, Microporous. Mesoporous. Mater. ***2021***, *319*, 111045. https://doi.org/10.1016/j.micromeso.2021.111045.

[35] P. Duxson, A. Fernández-Jiménez, J. L. Provis, G. C. Lukey, A. Palomo, J. S. van Deventer, Geopolymer technology: the current state of the art, J. Mater. Sci. ***2007***, *42*, 2917-2933. https://doi.org/10.1007/s10853-006-0637-z.

[36] H. K. Tchakouté, S. Kong, J. N. Y. Djobo, L. N. Tchadjié, D. Njopwouo, A comparative study of two methods to produce geopolymer composites from volcanic scoria and the role of structural water contained in the volcanic scoria on its reactivity, Ceram. Int. ***2015***, *41 :10*, 12568-12577. https://doi.org/10.1016/j.ceramint.2015.06.073.

[37] Sig, K. Y., Ahn, W. S. Isomorphous substitution of Fe3− in zeolite LTL, Microporous. Mater. ***(1997)***, *9:3-4*, 131-140. https://doi.org/10.1016/S0927-6513(96)00104-6.

[38] Z. Yunsheng, S. Wei, L. Zongjin, Composition design and microstructural characterization of calcined kaolin-based geopolymer cement, Appl. Clay. Sci. ***2010***, *47:3-4*, 271-275. https://doi.org/10.1016/j.clay.2009.11.002.

[39] J. Davidovits, L. Buzzi, P. Rocher, D. Gimeno, C. Marini, S. Tocco, Geopolymeric cement based on low-cost geologic materials. Results from the european research project geocistem. In Proceedings of the 2nd International Conference on Geopolymer ***(1999)***, *99*, 83-96.

[40] D. D. Burduhos-Nergis, P. Vizureanu, A. V. Sandu, B. Istrate, XRD and TG-DTA Analysis of Fly Ash Based Geopolymer Composite Reinforced with Recycled Glass Fibers, In International Conference on Innovative Research, Springer Nature Switzerland, ***(2023)***, 31-44. Cham: https://doi.org/10.1007/978-3-031-45964-1_4.

[41] C. Nobouassia Bewa, H. K. Tchakouté, D. Fotio, C. H. Rüscher, E. Kamseu, C. Leonelli, Water resistance and thermal behavior of metakaolin-phosphate-based geopolymer cements, J Asian. Ceram. Soc. ***2018***, *6:3*, 271-283. https://doi.org/10.1080/21870764.2018.1507660.

[42] E. Njoyim, P. Ghogomu, S. Laminsi, S. Nzali, A. Doubla, J. L. Brisset, Coupling gliding discharge treatment and catalysis by oyster shell powder for pollution abatement of surface waters, Indus. Eng. Chem. Res. ***2009***, *48:22*, 9773-9780. https://doi.org/10.1021/ie901118m.

[43] B. Cuiping, X. Xianfeng, G. Wenqi, F. Dexin, X. Mo, G. Zhongxue, X. Nian, Removal of rhodamine B by ozone-based advanced oxidation process, Desalination. ***2011***, *278:1-3*, 84-90. https://doi.org/10.1016/j.desal.2011.05.009.

[44] M. N. Ghazzal, H. Kebaili, M. Joseph, D. P. Debecker, P. Eloy, J. De Coninck, E. M. Gaigneaux, Photocatalytic degradation of Rhodamine 6G on mesoporous titania films: combined effect of texture and dye aggregation forms, Appl. Catal. B. ***2012***, *115*, 276-284. https://doi.org/10.1016/j.apcatb.2011.12.016.

[45] K. Hanna, T. Kone, G. Medjahdi, Synthesis of the mixed oxides of iron and quartz and their catalytic activities for the Fenton-like oxidation, Catal. Commun. ***2008***, *9:5*, 955-959. https://doi.org/10.1016/j.catcom.2007.09.035.

[46] K. Zhu, Y. Yao, X. Liang, Y. Yang, H.F. Garces, K. Yan, Recent progress in biochar-based photocatalysts for environmental remediation, Green Energy & Environ. ***2025***, *S2468-0257(25)00190-6*. https://doi.org/10.1016/j.gee.2025.07.006 .

[47] K. Zhu, R. Zhang, Y. Yao, M. Zhao, X. Huang, Z. Huang, Y. Yang, X. Liang, K. Yan, Oxygen vacancies engineering in iron-doped nickel molybdate nanorods to accelerate electron transfer for rapid organic pollutants removal, Sep. Purif. Technol. ***2025***, *372:1, 133391*. https://doi.org/10.1016/j.seppur.2025.133391.